JOC The Journal of Organic Chemistry

Article

pubs.acs.org/joc

5,20-Di(pyridin-2-yl)-[28]hexaphyrin(1.1.1.1.1.1): A Stable Hückel Antiaromatic Hexaphyrin Stabilized by Intramolecular Hydrogen Bonding and Protonation-Induced Conformational Twist To Gain Möbius Aromaticity

Koji Naoda,[†] Hirotaka Mori,[†] Juwon Oh,[‡] Kyu Hyung Park,[‡] Dongho Kim,*[,‡] and Atsuhiro Osuka*[,†]

[†]Department of Chemistry, Graduate School of Science, Kyoto University, Sakyo-ku, Kyoto 606-8502, Japan

[‡]Spectroscopy Laboratory for Functional π-Electronic Systems and Department of Chemistry, Yonsei University, Seoul 120-749, Korea

Supporting Information

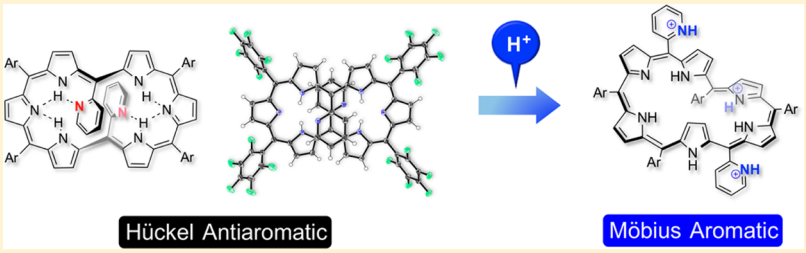

ABSTRACT: 5,20-Di(pyridin-2-yl)-[28]hexaphyrin(1.1.1.1.1.1) **7** was prepared and characterized as a stable Hückel antiaromatic molecule with a dumbbell-like structure stabilized by effective intramolecular hydrogen bonding interactions involving the 2-pyridyl nitrogen atoms. Pd(II) metalation of **7** afforded two bis-Pd(II) complexes, **9-syn** and **9-anti**, whose structures are rigidly held by Pd(II) coordination, rendering **9-syn** to be nonaromatic because of its highly distorted structure and **9-anti** to be Hückel antiaromatic because of its enforced planar dumbbell structure. In contrast, protonation of **7** with methanesulfonic acid (MSA) led to the formation of its triprotonated species $\mathbf{7H_3}$, which has been shown to take on twisted conformations with Möbius aromaticity in CH_2Cl_2, while the structure was held to be a planar rectangular conformation in the crystal. Excited-state dynamics were measured for **7**, $\mathbf{7H_3}$, **9-syn**, and **9-anti**, which indicated their electronic nature to be antiaromatic, aromatic, nonaromatic, and antiaromatic, respectively.

INTRODUCTION

In the past two decades, expanded porphyrins have attracted considerable interest in light of their intriguing optical, electrochemical, and structural properties.[1] These macrocycles have been demonstrated to exhibit various electronic states such as Hückel aromatic,[2] Hückel antiaromatic,[3] Möbius aromatic,[4] Möbius antiaromatic,[5] and stable radical states.[6] In addition, expanded porphyrins have been used as ligands for various metal ions[7] and anion-recognizing hosts.[8] We have entered into the chemistry of expanded porphyrins, because of our serendipitous finding of one-pot synthesis of a series of *meso*-aryl-substituted expanded porphyrins by the modified Lindsey method of porphyrin synthesis.[2] Characteristically, these *meso*-aryl-substituted expanded porphyrins possess cyclic conjugated electronic networks and conformational flexibility.[1f] The electronic properties of these macrocycles depend heavily upon their conformations, which are largely determined by their intramolecular NH···N hydrogen bonding interactions between imine-type and amine-type pyrroles. Therefore, conformations of expanded porphyrins can be readily changed by protonation,[9] metal coordination,[1,7] surrounding solvent,[1] temperature,[4a,b] and even molecular packing force in the solid state.[4b] For instance, palladium metalation of planar Hückel aromatic *meso*-hexakis(pentafluorophenyl) [26]hexaphyrin **1** afforded Möbius aromatic [28]hexaphyrin Pd(II) complex **2**, whose conformation is rigid at room temperature.[4c] In contrast, free base [28]hexaphyrin **3** exists in dynamic conformational equilibrium between Hückel and Möbius forms, and the Möbius conformation becomes predominant at low temperatures.[4b] Protonation of **3** induced dramatic conformational changes; monoprotonation increased the contribution of the Möbius conformation, and diprotonation gave rise to the formation of triangle Hückel antiaromatic hexaphyrin **3H**, probably because of the resultant intramolecular Coulombic repulsion.[9b] Recently, introduction of 2-imidazolyl substituents at positions 5 and 20 of hexaphyrin has been demonstrated to stabilize Hückel antiaromatic [28]hexaphyrin **4** through

Special Issue: 50 Years and Counting: The Woodward-Hoffmann Rules in the 21st Century

Received: June 15, 2015
Published: July 28, 2015

DOI: 10.1021/acs.joc.5b01348
J. Org. Chem. 2015, 80, 11726−11733

effective intramolecular hydrogen bonding interactions (Figure 1).[10]

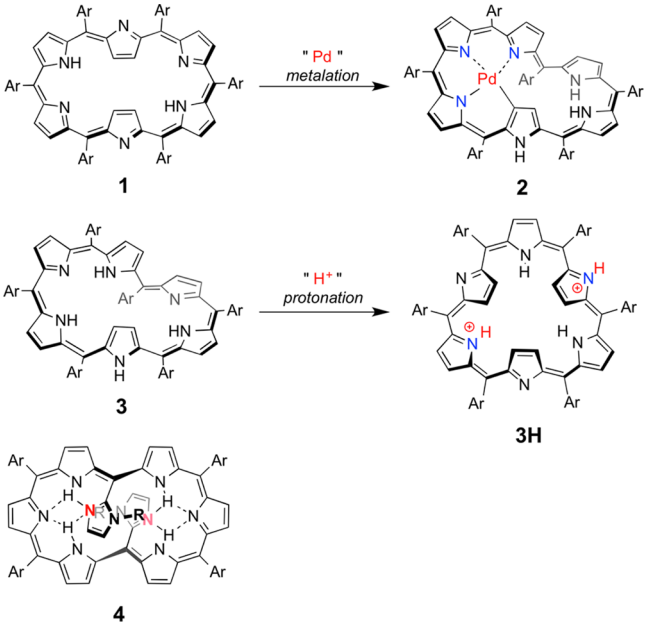

Figure 1. Schematic representations of compounds **1**–**4**. Ar = pentafluorophenyl. R = methyl or benzyl.

In this paper, we report the synthesis of 5,20-di(pyridin-2-yl)-substituted [28]hexaphyrin **7** with an expectation that intramolecular hydrogen bonding interactions involving the 2-pyridyl groups can stabilize a similar Hückel antiaromatic species. We also report on conformational and electronic changes of **7** upon its Pd(II) metalation and protonation.

RESULTS AND DISCUSSION

meso-5,20-Di(pyridin-2-yl)-substituted [28]hexaphyrin **7** was synthesized by the condensation reaction of tripyrrane **5** with 2-pyridinecarboxaldehyde **6** in the presence of 1.2 equiv of methanesulfonic acid (MSA) in CH_2Cl_2 followed by oxidation with 3 equiv of 2,3-dichloro-5,6-dicyano-1,4-benzoquinone (DDQ). After purification by silica gel column chromatography and recrystallization, [28]hexaphyrin **7** was obtained in 19% yield (Scheme 1). Here it is worth noting that only **7**, a reduced form of hexaphyrin, was isolated in this reaction, opposite to the trend that these reactions usually produce [26]hexaphyrins because of the final oxidation step. High-resolution electrospray ionization time-of-flight mass spectroscopy (HR-ESI-TOF MS) of **7** revealed the parent ion peak at m/z 1285.1830 (calcd m/z 1285.1877 for $C_{64}H_{25}N_8F_{20}$, $[M + H]^+$). The ^{1}H NMR spectrum of **7** at room temperature showed broad signals for the pyrrolic β-protons probably because of its slow conformational dynamics as compared with the ^{1}H NMR time scale. At −90 °C, its ^{1}H NMR spectrum showed two sharp singlets at 21.27 and 22.72 ppm in a 1/1 ratio because of the inner NH protons and six signals due to the pyrrolic outer β-protons in the range of 4.44−5.90 ppm, clearly indicating its antiaromatic character (Figure 5a). Four signals due to the 2-pyridyl groups are downfield shifted to the range of 8.63−12.13 ppm, reflecting a paratropic ring current of **7**. The nuclear independent chemical shift (NICS) value calculated by the GIAO method at the B3LYP/6-31G(d) level at the center of gravity of **7** is 9.40 ppm, thus supporting its antiaromaticity (Figure S31).[11] The UV/vis/NIR absorption spectrum of **7** showed three absorption bands at 345, 504, and 616 nm and a very weak absorption tail that reaches 1600 nm, which is characteristic of antiaromatic porphyrinoids because of the dark state (Figure 2).[12] The structure of **7** was determined by X-ray

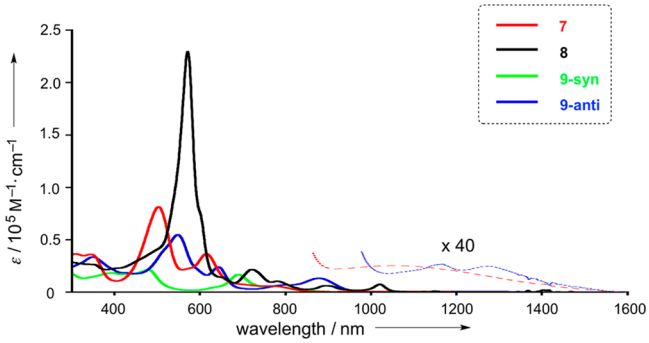

Figure 2. UV/vis/NIR absorption spectra of **7** (red line), **8** (black line), **9-syn** (yellow-green line), and **9-anti** (blue line) in CH_2Cl_2. The absorption bands of **7** (red dashed line) and **9-anti** (blue dashed line) in the NIR region were magnified 40-fold.

Scheme 1. Synthesis of [28]Hexaphyrin 7 and [26]Hexaphyrin 8 (Ar = pentafluorophenyl)

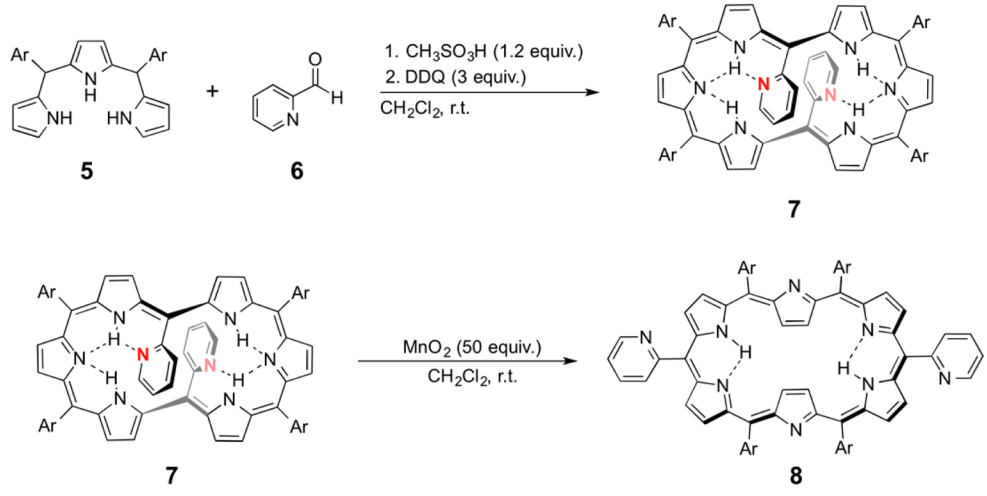

DOI: 10.1021/acs.joc.5b01348
J. Org. Chem. 2015, 80, 11726−11733

diffraction analysis, which revealed a planar dumbbell-like shape held by effective intramolecular hydrogen bonding interactions between the imine- and amine-type pyrroles and the 2-pyridyl groups (Figure 3a). It is conceivable that the incorporation of

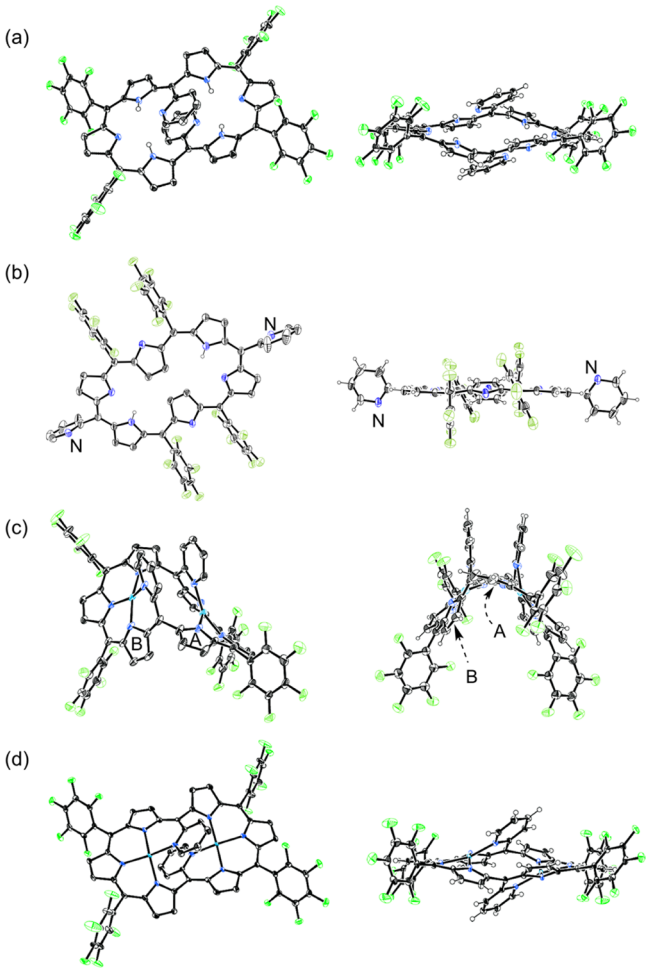

Figure 3. Crystal structures of (a) **7**, (b) **8**, (c) **9-syn**, and (d) **9-anti**: (left) perspective views and (right) side views. The thermal ellipsoids were scaled to the 50% probability level for **7** and **9-anti** and the 30% probability level for **8** and **9-syn**. Hydrogen atoms except for NHs in the perspective views and solvent molecules were omitted for the sake of clarity.

2-pyridyl groups helps this hexaphyrin **7** to take this conformation despite its antiaromatic destabilization, like the case of 5,20-di(imidazol-2-yl)-substituted [28]hexaphyrin.[10]

Oxidation of **7** with MnO_2 afforded [26]hexaphyrin **8** in 17% yield. Hexaphyrin **8** was, however, unstable and underwent slow decomposition in solution in the ambient atmosphere within a few hours. Thus, **8** was quickly separated by column chromatography and finally purified by recrystallization. Single crystals suitable for X-ray diffraction analysis were obtained from vapor diffusion of hexane into a $CHCl_3$ solution of **8** in a glovebox. The structure of **8** was revealed to be a planar rectangular shape bearing the 2-pyridyl groups at the shorter side (Figure 3b). The ^{1}H NMR spectrum of **8** exhibited two doublet peaks because of the outer β-protons at 9.40 and 9.20 ppm and one singlet signal for the inner β-proton at −2.54 ppm, indicating its aromatic character. The absorption spectrum of **8** displays a sharp Soret-like band at 572 nm and Q-like bands at 720, 781, 897, and 1021 nm, again supporting its aromaticity.

Because hexaphyrin **7** possesses two porphyrin-like NNNN cavities consisting of the tripyrromethene moiety and the 2-pyridyl group, we attempted its metalation with Pd(II) ion. When treated with 6 equiv of $Pd(OCOCF_3)_2$ in THF at 0 °C for 30 min, **7** was converted to bis-Pd(II) complexes **9-syn** and **9-anti** in 17 and 19% yields, respectively (Scheme 2). Although Pd(II) metalation of **7** proceeded smoothly at 0 °C, more than half of **7** decomposed under these conditions. The reaction at −40 °C gave low yields of **9-syn** and **9-anti**, and that at room temperature gave complicated reaction mixtures. In the HR-ESI-TOF mass spectra, both complexes exhibited the ion peaks almost at the same positions: m/z 1491.9504 for **9-syn** and m/z 1491.9579 for **9-anti** (calcd m/z 1491.9559 for $C_{64}H_{20}N_8F_{20}{}^{106}Pd_2$, $[M]^+$).

The structures of **9-syn** and **9-anti** were revealed by X-ray diffraction analysis to be structural isomers, where the two Pd(II) ions are bound to the three nitrogen atoms of the pyrroles and the one nitrogen atom of the 2-pyridyl group in a symmetric manner even though the locations of the 2-pyridyl substituents are different. Complex **9-syn** shows a highly distorted conformation, in which both of the two 2-pyridyl groups are located at the convex side. The dihedral angle between two planes of the pyrroles A and B is 80.4° (Figure 3c), which apparently interrupts cyclic π-conjugation of the hexaphyrin. In contrast, the structure of **9-anti** is roughly similar to that of free base **7**, in which two 2-pyridyl groups are on the opposite side of the hexaphyrin and the overall hexaphyrin conformation is kept rather planar, being favorable to cyclic π-conjugation (Figure 3d). The harmonic-oscillator model for aromaticity (HOMA)[13] values obtained from the crystal structures of **9-syn** and **9-anti** were 0.171 and 0.372, respectively, which also indicated more effective conjugation in **9-anti** as compared with that in **9-syn** (Figure S35). Total energies of **9-syn** [E_{tot}(**9-syn**)] and **9-anti** [E_{tot}(**9-anti**)] were obtained by DFT calculation at the B3LYP/6-31G(d)/LANL2DZ level (Table S4). It revealed that the difference in total energy between **9-syn** and **9-anti** [$\Delta E_{tot} = E_{tot}$(**9-syn**) − E_{tot}(**9-anti**)] is 12.67 kcal/mol, which indicated **9-anti** is much more thermodynamically stable than **9-syn** probably because of the smoother conjugation of **9-anti** as described above. Their

Scheme 2. Synthesis of Bis-Pd(II) Complexes 9-syn and 9-anti (Ar = pentafluorophenyl)

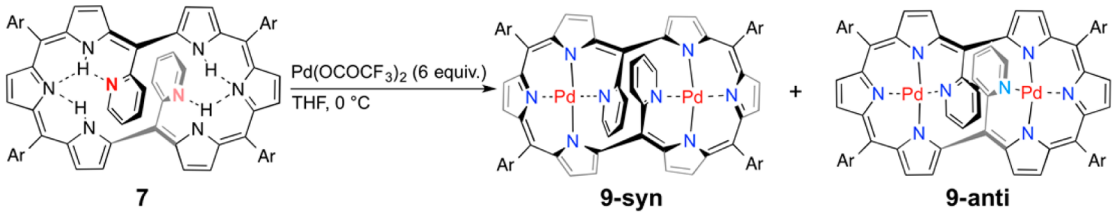

DOI: 10.1021/acs.joc.5b01348
J. Org. Chem. 2015, 80, 11726−11733

mutual interconversion was, however, not observed even when they were refluxed in toluene for 24 h, indicating their structural robustness.

The ^{1}H NMR spectrum of **9-syn** showed six signals due to the pyrrolic β-protons in the range of 5.75−6.85 ppm, suggesting its nonaromatic character. One of signals due to the 2-pyridyl groups was upfield shifted at 5.63 ppm because of the ring current of another pyridyl group located nearby in a parallel arrangement (Figure 3c). The UV/vis/NIR absorption spectrum of **9-syn** displays four broad bands at 395, 479, 690, and 776 nm (Figure 2). Conversely, the ^{1}H NMR spectrum of **9-anti** is similar to that of **7**, featuring six pyrrolic β-protons in the range of 4.68−5.87 ppm. The UV/vis/NIR absorption spectrum of **9-anti** shows four bands at 350, 548, 643, and 878 nm and a very weak absorption tail that reaches around 1600 nm (Figure 2), being similar to that of **7**, also indicating its antiaromaticity. NICS values at the center of gravities of **9-syn** and **9-anti** were calculated to be 1.41 and 9.22 ppm, respectively (Figures S32 and S33).

Electrochemical potentials were determined by cyclic voltammetry measurement in THF (Table 1). Characteristically, electrochemical HOMO−LUMO gaps (ΔE) of antiaromatic species **7** (1.13 eV) and **9-anti** (1.08 eV) are smaller than that of nonaromatic hexaphyrin **9-syn** (1.53 eV). DFT calculation gave ΔE values of 1.37 and 1.34 eV for **7** and **9-anti**, respectively, which are smaller than that of **9-syn** (2.08 eV).

Table 1. Redox Potentials ($E^{1/2}$) and Electrochemical HOMO−LUMO Gaps (ΔE) for Compounds 7, 9-syn, and 9-anti Measured in THF[a]

compound	$E^{1/2}_{ox3}$ (V)	$E^{1/2}_{ox2}$ (V)	$E^{1/2}_{ox1}$ (V)	$E^{1/2}_{red1}$ (V)	$E^{1/2}_{red2}$ (V)	ΔE[b] (eV)
7	–	0.15	−0.05	−1.18	−1.44	1.13
9-syn	0.86	0.37	0.12	−1.41	−1.69	1.53
9-anti	–	0.13	−0.19	−1.27	−1.67	1.08

[a]Potentials were determined vs ferrocene/ferrocenium ion. Electrolyte: NBu_4PF_6 (tetrabutylammonium hexafluorophosphate). Working electrode: glassy carbon. Counter electrode: Pt wire. Reference electrode: $Ag/AgClO_4$. [b]$\Delta E = E^{1/2}_{ox1} - E^{1/2}_{red1}$.

Finally, we examined the effect of protonation on **7** with MSA in CH_2Cl_2, because protonation may disrupt the intramolecular hydrogen bonding networks and hence cause conformational changes. Upon addition of MSA, the absorption band at 504 nm decreased and the absorption bands at 611, 858, and 961 nm increased. The spectral changes were saturated when 40 equiv of MSA was added (Figure 4). The final spectrum was characteristic of aromatic porphyrinoids bearing a Soret-like band and Q-like bands, suggesting the formation of twisted Möbius aromatic species. However, the broad Soret-like band indicated the presence of several conformers with regard to locations of *meso*-aryl substituents. Furthermore, in contrast to the nonfluorescence feature of **7**, the protonated species showed fluorescence emission in the 950−1250 nm region (Figure S16). A Job's plot for the protonation of **7** with MSA showed a maximum at 0.25 mole fraction (Figure 4, inset), indicating 1/3 stoichiometry of **7** and MSA, hence the formation of triprotonated species $\mathbf{7H_3}$ (Scheme 3a). Hill plots for the titration was also determined and provided an equilibrium constant (K) of 1.7×10^{14} M^{-3} (Figure S14).

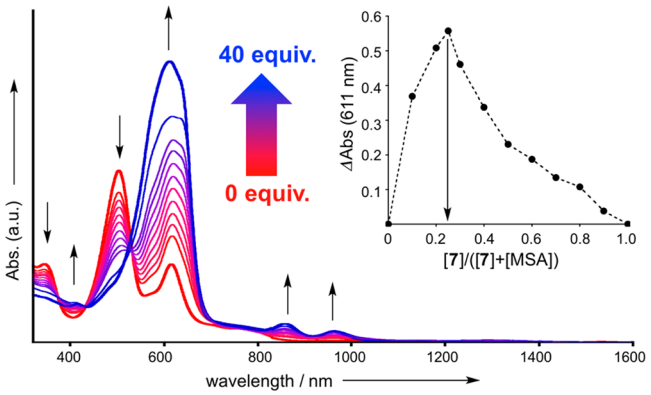

Figure 4. Spectroscopic titration of **7** with MSA in CH_2Cl_2. Ar = pentafluorophenyl. The inset is a Job's plot for the protonation of **7** at a constant total concentration (4.0×10^{-5} M).

When the protonation process was monitored via ^{1}H NMR spectroscopy in acetone-d_6 at −90 °C, the signals due to the inner NH protons at 21.27 and 22.72 ppm decreased, signals due to the inner protons emerged in the region from −3.42 to −2.15 ppm, and signals due to the pyrrolic outer protons including pyridyl groups downfield shifted to the range of 4.51−10.21 ppm (Figure 5b). These changes clearly indicated a diatropic ring current of $\mathbf{7H_3}$, although the spectrum became complicated because of the possible presence of several conformers of $\mathbf{7H_3}$. Temperature-dependent spectral changes of ^{1}H NMR spectra of $\mathbf{7H_3}$ were similar to those of hexakis(pentafluorophenyl)-[28]hexaphyrin **3**. Namely, the spectrum became partially broadened and could be observed only in the range of 7−10 ppm at room temperature, and at low temperatures, new signals due to the pyrrolic protons appeared in the region of 4−10 ppm and at <0 ppm (Figure 5b; see also Figures S11 and S12). These similarities again suggested twisted Möbius aromatic conformations for protonated species $\mathbf{7H_3}$.[4b]

Attempts have been made to obtain single crystals of the protonated species by vapor diffusion of diethyl ether into a mixture of CH_2Cl_2, MeOH, and MSA of **7**. X-ray crystallographic analysis of the obtained crystal revealed, however, a planar rectangular conformation bearing the 2-pyridyl groups at the longer side (Scheme 3b and Figure 6a,b). Although this planar structure may cause electronically unstable Hückel antiaromatic character, it is likely favored because of desirable packing with two methanesulfonate anions. This conformational difference between that in solution and the solid states is sometimes seen in hexaphyrins that we have reported because of their flexible nature.[4b] Interestingly, the two 2-pyridyl substituents were both protonated; thus, this protonated hexaphyrin is diprotonated species $\mathbf{7H_2}$ in the solid state (Scheme 3b). $\mathbf{7H_2}$ formed a hydrogen bond with the oxygen in the methansulfonate anion with a distance of 1.85 Å, hence being excluded from the intramolecular hydrogen bonding with the amine-type pyrroles. This finding underscores the importance of the hydrogen bonding of the 2-pyridyl groups with the amine-type pyrroles for the dumbbell-like conformation.

The optimized structure of $\mathbf{7H_3}$ has been calculated by the DFT method to be a twisted Möbius structure as shown in Figure 6c. The NICS value at the center of gravity of the calculated structure of $\mathbf{7H_3}$ was −9.83 ppm, in line with its aromatic character (Figure S34). A HOMA value calculated for

DOI: 10.1021/acs.joc.5b01348
J. Org. Chem. 2015, 80, 11726−11733

Scheme 3. Representations of Protonated Hexaphyrins[a]

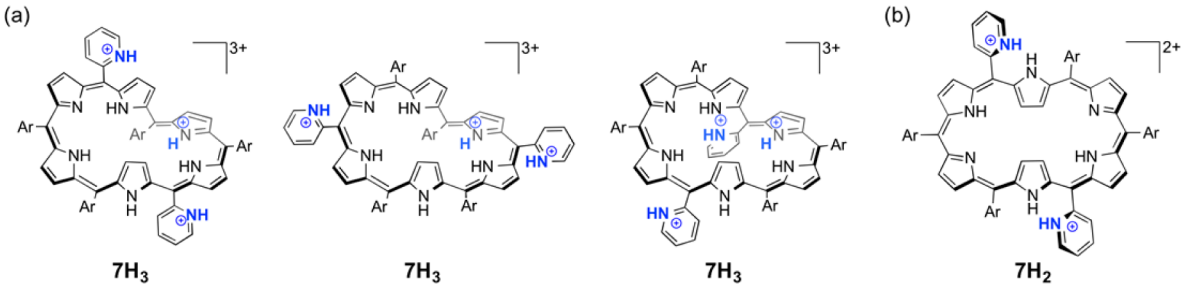

[a](a) Plausible protonated structures in solution ($7H_3$). (b) Protontaed structure in the solid state ($7H_2$). Ar = pentafluorophenyl.

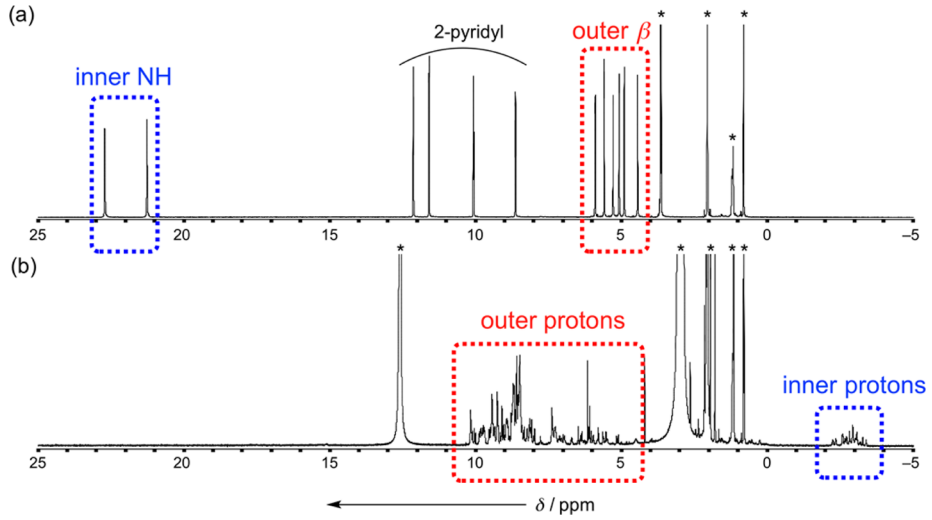

Figure 5. ^{1}H NMR spectra of (a) **7** and (b) $7H_3$ in acetone-d_6 at −90 °C. The asterisks denote residual solvents and MSA.

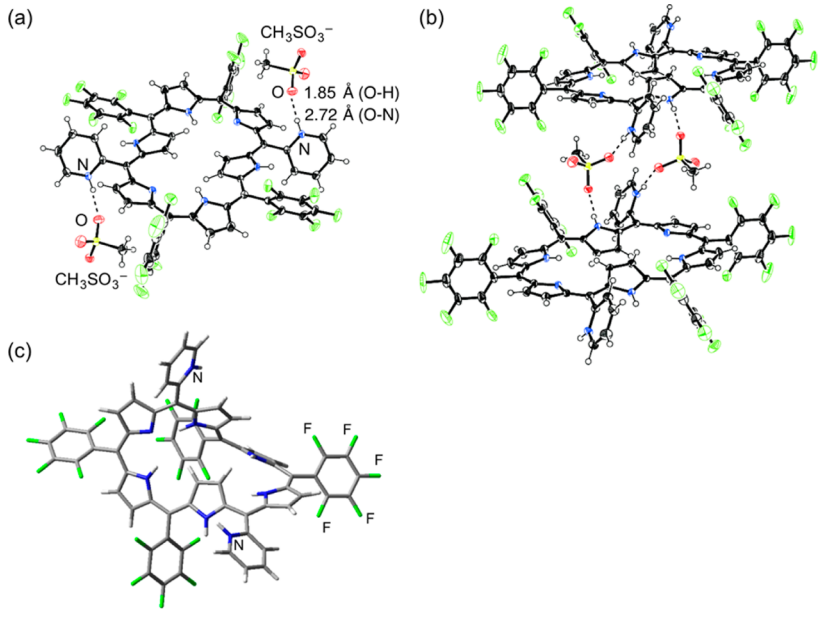

Figure 6. (a) Perspective view of the crystal structure of $7H_2$. (b) Partial packing structure of $7H_2$. The thermal ellipsoids were scaled to the 50% probability level. Other solvent molecules and methanesulfonic acids were omitted for the sake of clarity. (c) Optimized structure of $7H_3$ determined by DFT calculation using the B3LYP/6-31G(d) level.

$7H_3$ was 0.526. This value is larger than those of **7**, **9-syn**, and **9-anti**, thus suggesting a smoother conjugated circuit of $7H_3$ (Figure S35). These computational studies again suggested aromatic character of $7H_3$. Protonated hexaphyrin $7H_3$ was readily neutralized with triethylamine to give antiaromatic hexaphyrin **7**. These experiments showed the reversible interconversion between Hückel and Möbius topologies upon treatment with acid and base (Figure S15).

DOI: 10.1021/acs.joc.5b01348
J. Org. Chem. 2015, 80, 11726−11733

We have investigated the excited-state dynamics of **7**, **7H$_3$**, **9-syn**, and **9-anti** by femtosecond transient absorption (TA) measurements (Figures S17−S20). The decay profile of TA spectra of **7** showed double-exponential decay with two time constants of 1 and 17 ps. This feature indicates the presence of a NIR dark state, which leads to the characteristic excited-state dynamics of antiaromatic porphyrinoids.[12] Because the dark state acts as a ladder in the decay processes, **7** displayed the fast internal conversion (IC) to the dark S_1 state and subsequent decay to the ground state, which correspond to decay time constants of 1 and 17 ps, respectively. Moreover, the TA spectra of **7** displayed the relatively weak ground-state bleaching (GSB) band at 617 nm and intense excited-state absorption (ESA) bands on both sides of GSB band. These temporal and spectral observations represent the antiaromatic nature of **7**. On the other hand, **7H$_3$** showed the TA spectra that are radically different from those of **7**. The S_1-state lifetime of **7H$_3$** was significantly increased to 125 ps, which is well matched by its fluorescence behavior.[12] In addition, the distinct GSB bands at 575 and 630 nm compared to the broad ESA band over 670 nm were observed in the TA spectra of **7H$_3$**. These spectral features are in accordance with the aromatic character of **7H$_3$**.[12] It was found that the excited-state dynamics of **9-syn** reflects the nonaromatic nature as expected by the highly distorted structure from X-ray crystallography. The TA spectra of **9-syn** were globally analyzed to include two principal species, which decayed with two time constants of 7 ps and a long component. Because the heavy-atom effect of palladium ion of **9-syn** gives rise to an efficient intersystem crossing (ISC) process, the two decay processes are most probably assigned as the lifetimes of the S_1 and T_1 states. This simple excited-state dynamics, composed of the short S_1-state and long T_1-state decay processes, shows its obvious nonaromatic character. Similar to those of **9-syn**, the TA spectra of **9-anti** also displayed the efficient ISC process as a result of the heavy-atom effect of palladium ion. However, the TA spectra of **9-anti** decayed with two time constants of 0.3 and 22 ps as well as the long decay component. As in the case of **7**, these two decay processes can be assigned as the fast IC process and short S_1-state lifetime, which reflects the presence of the NIR dark state. In other words, the fast double-exponential decay is the manifestation of Hückel antiaromaticity of **9-anti**, while the ISC process facilitated by palladium ion causes the formation of a long-lasting population in the T_1 state.

SUMMARY

The dumbbell-like conformation of *meso*-5,20-di(pyridin-2-yl)-substituted [28]hexaphyrin **7** was stabilized by the effective intramolecular hydrogen bonding interactions involving the 2-pyridyl substituents despite its antiaromatic character. Palladium metalation to **7** afforded two bis-Pd(II) complexes, **9-syn** and **9-anti**. The structures of **9-syn** and **9-anti** are rigidly held by Pd(II) ion coordination, which makes these complexes a highly distorted nonaromatic molecule and a dumbbell-like antiaromatic molecule, respectively. The protonation of **7** with MSA, however, led to the formation of **7H$_3$**, which has been shown to take on twisted conformations with Möbius aromaticity in CH_2Cl_2, although **7H$_3$** has taken on a planar rectangular conformation **7H$_2$** in the crystal. The ultrafast excited-state dynamics of these hexaphyrins have been measured, which also supports the assignments given above. Further investigation to introduce such hydrogen bonding acceptor substituents into expanded porphyrins is ongoing in our laboratory and will be reported elsewhere.

EXPERIMENTAL SECTION

General Experimental Methods. All reagents were of the commercial reagent grade and were used without further purification. Silica gel, alumina, Florisil, and Celite are commercially available and were used for column chromatography. UV/vis/NIR absorption spectra were recorded on a UV spectrometer. ^{1}H, ^{19}F, and ^{13}C NMR spectra were recorded on a spectrometer (operating as 600.17 MHz for ^{1}H, 564.73 MHz for ^{19}F, and 150.91 MHz for ^{13}C) using the residual solvents as the internal references for ^{1}H (δ 7.26 in $CHCl_3$, δ 2.05 in acetone, and δ 6.97 in toluene) and ^{13}C (δ 29.87 in acetone and δ 137.48 in toluene) and hexafluorobenzene as the external reference for ^{19}F (δ −162.9). High-resolution electrospray ionization time-of-flight mass spectroscopy (HR-ESI-TOF MS) was conducted by using the positive mode for an acetonitrile solution of samples. Redox potentials were measured by cyclic voltammetry on an electrochemical analyzer. Crystallographic data were collected at −180 °C by using graphite-monochromated Cu Kα radiation (λ = 1.54187 Å). The structures were determined by direct methods and refined by the full-matrix least-squares technique. The femtosecond transient absorption (fs-TA) spectra measured with a spectrometer consisting of two independently tunable homemade optical parametric amplifiers (OPAs) pumped by a regeneratively amplified Ti:sapphire laser system operating at a repetition rate of 1 kHz and an optical detection system.

5,20-Di(pyridin-2-yl)-Substituted [28]Hexaphyrin-(1.1.1.1.1.1) 7. To a solution of 2-pyridinecarboxaldehyde (**6**) (102 μL, 1.0 equiv) in CH_2Cl_2 (100 mL) was added MSA in CH_2Cl_2 (2.5 M, 0.52 mL, 1.2 equiv), and the resulting solution was stirred for 10 min at room temperature. A solution of 5,10-bis(pentafluorophenyl)-tripyrromethane (**5**) (600 mg, 0.54 mmol) in CH_2Cl_2 (10 mL) was added at once to this mixture. The reaction mixture was stirred for 2 h in the dark at the same temperature. DDQ (740 mg, 3 equiv) was then added, and the resulting solution was stirred for 30 min. The reaction mixture was passed through an alumina column using a 10/1 mixture of CH_2Cl_2 and MeOH as an eluent. The solvent was removed under reduced pressure to leave residue, which was purified by silica gel column chromatography using a mixture of CH_2Cl_2 and hexane (1/2) as an eluent. The first gray fraction was collected and recrystallized from a mixture of CH_2Cl_2 and hexane to give **7** (132 mg, 0.10 mmol, 19%) as dark green solids. Single crystals suitable for X-ray crystallographic analysis were obtained by vapor diffusion of hexane into a CH_2Cl_2 solution of **7**. The protonated structure of **7H$_2$** was obtained by vapor diffusion of diethyl ether into a solution of **7** in a mixture of CH_2Cl_2, MeOH, and MSA.

7: ^{1}H NMR (acetone-d_6, −90 °C, 600.17 MHz) δ 22.72 (s, 2H, NH), 21.27 (s, 2H, NH), 12.13 (d, J = 7.8 Hz, 2H, pyridyl), 11.60 (d, J = 4.1 Hz, 2H, pyridyl), 10.06 (d, J = 8.3 Hz, 2H, pyridyl), 8.63 (d, J = 1.9 Hz, 2H, pyridyl), 5.90 (d, J = 4.1 Hz, 2H, β-H), 5.58 (d, J = 4.6 Hz, 2H, β-H), 5.28 (d, J = 4.8 Hz, 2H, β-H), 5.07 (d, J = 4.1 Hz, 2H, β-H), 4.90 (brs, 2H, β-H), 4.44 (brs, 2H, β-H); ^{19}F NMR (acetone-d_6, −90 °C, 564.73 MHz) δ −133.74 (d, J = 21.7 Hz, 2F, o-C_6F_5), −141.58 (d, J = 21.7 Hz, 2F, o-C_6F_5), −141.97 (d, J = 21.7 Hz, 2F, o-C_6F_5), −142.05 (d, J = 21.7 Hz, 2F, o-C_6F_5), −156.74 (t, J = 17.3 Hz, 2F, p-C_6F_5), −158.20 (t, J = 17.3 Hz, 2F, p-C_6F_5), −162.61 (t, J = 17.3 Hz, 2F, m-C_6F_5), −163.03 (t, J = 17.3 Hz, 2F, m-C_6F_5), −163.72 (t, J = 17.3 Hz, 2F, m-C_6F_5), −164.00 (t, J = 17.3 Hz, 2F, m-C_6F_5); ^{13}C NMR (acetone-d_6, −90 °C, 150.91 MHz) δ 172.5, 163.5, 157.3, 155.9, 153.6, 146.6, 145.2, 141.0, 140.4, 137.1, 134.0, 130.1, 126.5, 126.2, 124.0, 119.8, 117.4, 110.5, 109.8, and 96.4 (the signals for pentafluorophenyl carbons were not observed clearly because of their weak intensity); UV/vis/NIR (CH_2Cl_2) λ_{max} [ε (M^{-1} cm^{-1})] 345 (36200), 504 (81500), 616 (36500) nm; HR-ESI-TOF MS m/z 1285.1830 (calcd m/z 1285.1877 for $C_{64}H_{25}N_8F_{20}$ $[M + H]^+$).

7H$_3$ (**7** with 40 equiv of MSA): ^{1}H NMR (acetone-d_6, −90 °C, 600.17 MHz) δ 10.21 (d, J = 7.8 Hz), 10.17 (d, J = 7.2 Hz), 10.13 (d, J = 8.2 Hz), 10.04 (d, J = 7.8 Hz), 10.00 (d, J = 7.2 Hz), 9.90 (m), 9.83

DOI: 10.1021/acs.joc.5b01348
J. Org. Chem. 2015, 80, 11726−11733

(m), 9.78 (d, J = 7.2 Hz), 9.73 (m), 9.70 (m), 9.57 (m), 9.51 (m), 9.45 (m), 9.37 (m), 9.29 (m), 9.17 (m), 9.12 (m), 9.09 (m), 9.06 (m), 8.96 (m), 8.90 (m), 8.79 (m), 8.71 (m), 8.52 (m), 8.33 (br), 8.24 (m), 8.17 (m), 8.13 (br), 8.06 (m), 8.02 (m), 7.98 (br), 7.84 (m), 7.41(m), 7.30 (br), 7.01 (m), 6.97 (br), 6.71 (br), 6.50 (m), 6.41 (m), 6.37 (m), 6.32 (m), 6.26 (m), 6.17 (m), 6.15 (m), 6.08 (m), 5.96 (br), 5.84 (m), 5.60 (m), 5.57 (m), 5.45 (br), 5.14 (m), 4.51 (br), −2.15 (m), −2.30 (m), −2.56 (m), −2.59 (m), −2.63 (m), −2.68 (m), −2.78 (m), −2.90 (m), −2.94 (m), −3.02 (m), −3.10 (m), −3.15 (m), −3.19 (m), −3.33 (m), −3.42 (m); ^{19}F NMR (acetone-d_6, −90 °C, 564.73 MHz) δ −137.67 (m, o-C_6F_5), −139.32 (m, o-C_6F_5), −139.50 (m, o-C_6F_5), −140.33 (m, o-C_6F_5), −141.41 (br, o-C_6F_5), −141.61 (br, o-C_6F_5), −142.56 (m, o-C_6F_5), −142.95 (m, o-C_6F_5), −143.21 (m, o-C_6F_5), −143.84 (br, o-C_6F_5), −151.52 (br, p-C_6F_5), −152.54 (m, p-C_6F_5), −153.86 (m, p-C_6F_5), −161.81 (br, m-C_6F_5), −162.03 (br, m-C_6F_5), −162.47 (br, m-C_6F_5), −162.87 (m, m-C_6F_5), −163.40 (m, m-C_6F_5), −163.90 (br, m-C_6F_5), −164.29 (br, m-C_6F_5), −164.48 (m, m-C_6F_5), −164.99 (m, m-C_6F_5), −166.04 (br, m-C_6F_5); ^{13}C NMR (acetone-d_6, −90 °C, 150.91 MHz) δ 156.4, 148.7 (br), 148.1 (br), 146.5 (br), 144.0 (br), 142.4 (br), 140.2, 139.9, 139.0 (br), 138.2 (br), 137.3 (br), 126.0 (br), 123.8, 123.7, 123.5, 114.8 (br), 113.1 (br), 112.3 (br), 110.7 (br), 103.6 (br) (the NMR spectra of **7H$_3$** were complicated because of the several conformers of **7H$_3$**; thus, it is hard to assign and integrate peaks correctly); UV/vis/NIR (CH_2Cl_2) λ_{max} 611 (Soret-like band), 858 (Q-like band), 961 (Q-like band) nm.

5,20-Di(pyridin-2-yl)-Substituted [26]-Hexaphyrin(1.1.1.1.1.1) 8. To a solution of **7** (15 mg, 11.7 μmol) in CH_2Cl_2 (5 mL) was added MnO_2 (30 mg, 50 equiv), and the resulting solution was stirred until **7** was completely consumed. After the reaction had reached completion, the excess amount of MnO_2 was removed by passing the mixture through a short Celite column. The residue was purified by silica gel column chromatography using CH_2Cl_2 and AcOEt (20/1) as an eluent. A violet fraction was collected and dried. Recrystallization from CH_2Cl_2 and hexane gave title compound **8** (2.6 mg, 2.0 μmol, 17%). Single crystals suitable for X-ray crystallographic analysis were obtained by vapor diffusion of hexane into a $CHCl_3$ solution of **8** in a glovebox.

8: ^{1}H NMR ($CDCl_3$, 25 °C, 600.17 MHz) δ 9.40 (d, J = 4.6 Hz, 4H, outer β-H), 9.26 (d, J = 5.0 Hz, 2H, pyridyl), 9.20 (d, J = 4.6 Hz, 4H, outer β-H), 8.44 (d, J = 7.3 Hz, 2H, pyridyl), 8.29 (t, J = 5.9 Hz, 2H, pyridyl), 7.88 (t, J = 5.0 Hz, 2H, pyridyl), − 2.12 (br, 2H NH), −2.54 (s, 4H inner β-H); ^{19}F NMR ($CDCl_3$, 25 °C, 564.73 MHz) δ −136.88 (d, J = 21.7 Hz, 8F, o-C_6F_5), −153.34 (t, J = 21.7 Hz, 4F, p-C_6F_5), −163.27 (t, J = 17.3 Hz, 8F, m-C_6F_5) (^{13}C NMR could not be conducted because of the instability of **8** in solution for a long time measurement); UV/vis/NIR (CH_2Cl_2) λ_{max} [ε (M^{-1} cm^{-1})] 572 (229000), 720 (21500), 781 (10500), 897 (6100), 1021 (7500) nm; HR-ESI-TOF MS m/z 1283.1681 (calcd m/z 1283.1721 for $C_{64}H_{23}N_8F_{20}$ $[M + H]^+$).

Palladium(II) Complexes of 5,20-Di(pyridin-2-yl)-Substituted [28]Hexaphyrin, 9-syn and 9-anti. To a solution of **7** (32 mg, 25 μmol) in THF (3 mL) was added a solution of palladium bis(trifluoroacetate) (50 mg, 150 μmol, 6 equiv) in THF at 0 °C. After being stirred for 30 min at 0 °C, the reaction mixture was passed through a short Florisil column using CH_2Cl_2 as an eluent, and the solvent was removed to leave residue, which was purified by silica gel column chromatography using a 1/2 mixture of CH_2Cl_2 and hexane to give **9-anti** (7.0 mg, 4.7 μmol, 19%) as the first red fraction and **9-syn** (6.4 mg, 4.3 μmol, 17%) as the second yellow-green fraction. Single crystals suitable for X-ray crystallographic analysis were obtained by vapor diffusion of octane into a toluene solution of **9-syn** and vapor diffusion of hexane into a $CHCl_3$ solution of **9-anti**.

9-syn: ^{1}H NMR (toluene-d_8, 25 °C, 600.17 MHz) δ 7.87 (d, J = 5.5 Hz, 2H, pyridyl), 7.16 (d, J = 8.3 Hz, 2H, pyridyl), 6.85 (d, J = 3.7 Hz, 2H, β-H), 6.83 (d, J = 5.0 Hz, 2H, β-H), 6.70 (d, J = 3.7 Hz, 2H, β-H), 6.40 (d, J = 5.0 Hz, 2H, β-H), 6.36 (t, J = 7.2 Hz, 2H, pyridyl), 6.30 (d, J = 5.0 Hz, 2H, β-H), 5.75 (d, J = 5.5 Hz, 2H, β-H), 5.63 (t, J = 6.9 Hz, 2H, pyridyl); ^{19}F NMR (toluene-d_8, 25 °C, 564.23 MHz) δ −136.02 (d, J = 17.3 Hz, 2F, o-C_6F_5), −139.02 (d, J = 17.3 Hz, 2F, o-C_6F_5), −139.32 (d, J = 21.7 Hz, 2F, o-C_6F_5), −139.96 (d, J = 30.4 Hz, 2F, o-C_6F_5), −152.56 (t, J = 22.1 Hz, 2F, p-C_6F_5), −154.34 (t, J = 22.0 Hz, 2F, p-C_6F_5), −161.38 (t, J = 22.3 Hz, 4F, m-C_6F_5), −162.13 (t, J = 21.5 Hz, 2F, m-C_6F_5), −162.39 (t, J = 20.3 Hz, 2F, m-C_6F_5); ^{13}C NMR (toluene-d_8, 25 °C, 150.91 MHz) δ 153.9, 153.8, 153.4, 151.9, 148.2, 146.5, 139.7, 138.9, 134.0, 133.2, 131.4, 130.6, 124.0, 122.5, 121.9, 120.3, 119.3, 118.5, 118.0, 96.1 (the signals for pentafluorophenyl carbons were not observed clearly because of their weak intensity); UV/vis/NIR (CH_2Cl_2) λ_{max} [ε (M^{-1} cm^{-1})] 395 (18400), 479 (21300), 690 (16900), 776 (5300) nm; HR-ESI-TOF MS m/z 1491.9504 (calcd m/z 1491.9559 for $C_{64}H_{20}N_8F_{20}{}^{106}Pd_2$ $[M]^+$).

9-anti: ^{1}H NMR (acetone-d_6, −80 °C, 600.17 MHz) δ 13.20 (d, J = 5.5 Hz, 2H, pyridyl), 12.46 (d, J = 7.8 Hz, 2H, pyridyl), 10.80 (t, J = 7.4 Hz, 2H, pyridyl), 9.49 (t, J = 5.5 Hz, 2H, pyridyl), 5.87 (d, J = 5.5 Hz, 2H, β-H), 5.27 (d, J = 5.5 Hz, 2H, β-H), 5.25 (d, J = 5.5 Hz, 2H, β-H), 4.81 (d, J = 4.6 Hz, 2H, β-H), 4.78 (d, J = 3.7 Hz, 2H, β-H), 4.68 (d, J = 4.1 Hz, 2H, β-H); ^{19}F NMR (acetone-d_6, −80 °C, 564.73 MHz) δ −139.07 (d, J = 21.7 Hz, 2F, o-C_6F_5), −141.82 (d, J = 26.0 Hz, 2F, o-C_6F_5), −142.13 (d, J = 21.6 Hz, 2F, o-C_6F_5), −142.85 (d, J = 21.7 Hz, 2F, o-C_6F_5), −156.98 (t, J = 21.7 Hz, 2F, p-C_6F_5), −158.37 (t, J = 21.7 Hz, 2F, p-C_6F_5), −162.56 (t, J = 21.6 Hz, 2F, m-C_6F_5), −163.24 (t, J = 21.7 Hz, 2F, m-C_6F_5), −163.83 (t, J = 17.3 Hz, 2F, m-C_6F_5), −163.95 (t, J = 21.7 Hz, 2F, m-C_6F_5) (^{13}C NMR could not be conducted because of the poor solubility of **9-anti**); UV/vis/NIR (CH_2Cl_2) λ_{max} [ε (M^{-1} cm^{-1})] 350 (33600), 548 (54800), 643 (24100), 878 (13300) nm; HR-ESI-TOF MS m/z 1491.9579 (calcd m/z 1491.9559 for $C_{64}H_{20}N_8F_{20}{}^{106}Pd_2$ $[M]^+$).

CCDC entry 1405973 for **7**, 1405975 for **8**, 1405976 for **9-syn**, 1405977 for **9-anti**, and 1405978 for **7H$_2$** contain the supplementary crystallographic data for this paper. These data can be obtained free of charge from The Cambridge Crystallographic Data Centre via www.ccdc.cam.ac.uk/data_request/cif.

■ ASSOCIATED CONTENT

Supporting Information

The Supporting Information is available free of charge on the ACS Publications website at DOI: 10.1021/acs.joc.5b01348.

NMR spectra, HR-ESI-TOF mass spectra, details of absorption spectroscopic titration, cyclic voltammograms, X-ray crystallographic details, and results of DFT calculations and TA spectra (PDF)
Crystallographic data of **7** (CIF)
Crystallographic data of **8** (CIF)
Crystallographic data of **9-syn** (CIF)
Crystallographic data of **9-anti** (CIF)
Crystallographic data of **7H$_2$** (CIF)

■ AUTHOR INFORMATION

Corresponding Authors

*E-mail: dongho@yonsei.ac.kr.
*E-mail: osuka@kuchem.kyoto-u.ac.jp.

Notes

The authors declare no competing financial interest.

■ ACKNOWLEDGMENTS

The work at Kyoto was supported by JSPS KAKENHI Grants 25220802 and 25620031. K.N. and H.M. acknowledge a JSPS Fellowship for Young Scientists. The work at Yonsei University was supported by the Global Research Laboratory Program (2013K1A1A2A02050183) by the Ministry of Science, ICT & Future, Korea.

■ REFERENCES

(1) (a) Jasat, A.; Dolphin, D. *Chem. Rev.* **1997**, *97*, 2267. (b) Lash, T. D. *Angew. Chem., Int. Ed.* **2000**, *39*, 1763. (c) Chandrashekar, T. K.; Venkatraman, S. *Acc. Chem. Res.* **2003**, *36*, 676. (d) Sessler, J. L.;

DOI: 10.1021/acs.joc.5b01348
J. Org. Chem. 2015, 80, 11726−11733

Seidel, D. *Angew. Chem., Int. Ed.* **2003**, *42*, 5134. (e) Stępień, M.; Sprutta, N.; Latos-Grażyński, L. *Angew. Chem., Int. Ed.* **2011**, *50*, 4288. (f) Saito, S.; Osuka, A. *Angew. Chem., Int. Ed.* **2011**, *50*, 4342. (g) Pawlicki, M.; Latos-Grażyński, L. *Chem. - Asian J.* **2015**, *10*, 1438.
(2) Shin, J.-Y.; Furuta, H.; Yoza, K.; Igarashi, S.; Osuka, A. *J. Am. Chem. Soc.* **2001**, *123*, 7190.
(3) Reddy, J. S.; Mandal, S.; Anand, V. G. *Org. Lett.* **2006**, *8*, 5541.
(4) (a) Stępień, M.; Latos-Grażyński, L.; Sprutta, N.; Chwalisz, P.; Szterenberg, L. *Angew. Chem., Int. Ed.* **2007**, *46*, 7869. (b) Sankar, J.; Mori, S.; Saito, S.; Rath, H.; Suzuki, M.; Inokuma, Y.; Shinokubo, H.; Suk Kim, K.; Yoon, Z. S.; Shin, J.-Y.; Lim, J. M.; Matsuzaki, Y.; Matsushita, O.; Muranaka, A.; Kobayashi, N.; Kim, D.; Osuka, A. *J. Am. Chem. Soc.* **2008**, *130*, 13568. (c) Tanaka, Y.; Saito, S.; Mori, S.; Aratani, N.; Shinokubo, H.; Shibata, N.; Higuchi, Y.; Yoon, Z. S.; Kim, K. S.; Noh, S. B.; Park, J. K.; Kim, D.; Osuka, A. *Angew. Chem., Int. Ed.* **2008**, *47*, 681.
(5) (a) Pacholska-Dudziak, E.; Skonieczny, J.; Pawlicki, M.; Szterenberg, L.; Ciunik, Z.; Latos-Grażyński, L. *J. Am. Chem. Soc.* **2008**, *130*, 6182. (b) Higashino, T.; Lim, J. M.; Miura, T.; Saito, S.; Shin, J.-Y.; Kim, D.; Osuka, A. *Angew. Chem., Int. Ed.* **2010**, *49*, 4950.
(6) (a) Koide, T.; Furukawa, K.; Shinokubo, H.; Shin, J.-Y.; Kim, K. S.; Kim, D.; Osuka, A. *J. Am. Chem. Soc.* **2010**, *132*, 7246. (b) Gopalakrishna, T. Y.; Reddy, J. S.; Anand, V. G. *Angew. Chem., Int. Ed.* **2014**, *53*, 10984. (c) Hisamune, Y.; Nishimura, K.; Isakari, K.; Ishida, M.; Mori, S.; Karasawa, S.; Kato, T.; Lee, S.; Kim, D.; Furuta, H. *Angew. Chem., Int. Ed.* **2015**, *54*, 7323.
(7) Sessler, J. L.; Tomat, E. *Acc. Chem. Res.* **2007**, *40*, 371.
(8) (a) Sessler, J. L.; Mody, T. D.; Ford, D. A.; Lynch, V. *Angew. Chem., Int. Ed. Engl.* **1992**, *31*, 452. (b) Sessler, J. L.; Andrievsky, A.; Král, V.; Lynch, V. *J. Am. Chem. Soc.* **1997**, *119*, 9385. (c) Sessler, J. L.; Davis, J. M. *Acc. Chem. Res.* **2001**, *34*, 989. (d) Seidel, D.; Lynch, V.; Sessler, J. L. *Angew. Chem., Int. Ed.* **2002**, *41*, 1422. (e) Köhler, T.; Seidel, D.; Lynch, V.; Arp, F. O.; Ou, Z.; Kadish, K. M.; Sessler, J. L. *J. Am. Chem. Soc.* **2003**, *125*, 6872.
(9) (a) Stępień, M.; Szyszko, B.; Latos-Grażyński, L. *J. Am. Chem. Soc.* **2010**, *132*, 3140. (b) Ishida, S.; Higashino, T.; Mori, S.; Mori, H.; Aratani, N.; Tanaka, T.; Lim, J. M.; Kim, D.; Osuka, A. *Angew. Chem., Int. Ed.* **2014**, *53*, 3427.
(10) Mori, H.; Sung, Y. M.; Lee, B. S.; Kim, D.; Osuka, A. *Angew. Chem., Int. Ed.* **2012**, *51*, 12459.
(11) (a) Schleyer, P. v. R.; Maerker, C.; Dransfeld, A.; Jiao, H.; Hommes, N. J. R. v. E. *J. Am. Chem. Soc.* **1996**, *118*, 6317. (b) Chen, Z.; Wannere, C. S.; Corminboeuf, C.; Puchta, R.; Schleyer, P. v. R. *Chem. Rev.* **2005**, *105*, 3842.
(12) Shin, J.-Y.; Kim, K. S.; Yoon, M.-C.; Lim, J. M.; Yoon, Z. S.; Osuka, A.; Kim, D. *Chem. Soc. Rev.* **2010**, *39*, 2751.
(13) Krygowski, T. M. *J. Chem. Inf. Model.* **1993**, *33*, 70.

DOI: 10.1021/acs.joc.5b01348
J. Org. Chem. 2015, 80, 11726−11733